Dentomaxillofacial Radiology (2022) 51, 20220044
© 2022 The Authors. Published by the British Institute of Radiology under the terms of the Creative Commons Attribution-NonCommercial 4.0 Unported License http://creativecommons.org/licenses/by-nc/4.0/, which permits unrestricted non-commercial reuse, provided the original author and source are credited.

birpublications.org/dmfr

RESEARCH ARTICLE

High-resolution ultrasonography of gingival biomarkers for periodontal diagnosis in healthy and diseased subjects

[1]Colman A Moore, [2]Jane K Law, [1]Maurice Retout, [2]Christopher T Pham, [2]Kai Chiao J Chang, [2]Casey Chen and [1,3,4]Jesse V Jokerst

[1]Department of NanoEngineering, University of California, San Diego, 9500 Gilman Drive. La Jolla, CA, USA; [2]Herman Ostrow School of Dentistry, University of Southern California, 925 West 34th Street, Los Angeles, CA, USA; [3]Materials Science Program, University of California, San Diego, 9500 Gilman Drive. La Jolla, CA, USA; [4]Department of Radiology, University of California, San Diego, 9500 Gilman Drive. La Jolla, CA, USA

Objective: To determine the capacity of ultrasonographic image-based measurements of gingival height and alveolar bone level for monitoring periodontal health and disease.
Methods: Sixteen subjects were recruited from patients scheduled to receive dental care and classified as periodontally healthy (n = 10) or diseased (n = 6) according to clinical guidelines. A 40-MHz ultrasound system was used to measure gingival recession, gingival height, alveolar bone level, and gingival thickness from 66 teeth for comparison to probing measurements of pocket depth and clinical attachment level. Interexaminer variability and comparison between ultrasound measurements and probing measurements was performed via Bland-Altman analysis.
Results: Gingival recession and its risk in non-recessed patients could be determined via measurement of the supra- and subgingival cementoenamel junction relative to the gingival margin. Interexaminer bias for ultrasound image analysis was negligible (<0.10 mm) for imaged gingival height (iGH) and 0.45 mm for imaged alveolar bone level (iABL). Diseased subjects had significantly higher imaging measurements (iGH, iABL) and clinical measurements (probing pocket depth, clinical attachment level) than healthy subjects ($p < 0.05$). Subtraction of the average biologic width from iGH resulted in 83% agreement (≤1 mm difference) between iGH and probing pocket depth measurements.
Conclusions: Ultrasonography has an equivalent diagnostic capacity as gold-standard physical probing for periodontal metrics while offering more detailed anatomical information.
Dentomaxillofacial Radiology (2022) **51**, 20220044. doi: 10.1259/dmfr.20220044

Cite this article as: Moore CA, Law JK, Retout M, Pham CT, Chang KCJ, Chen C, et al. High-resolution ultrasonography of gingival biomarkers for periodontal diagnosis in healthy and diseased subjects. *Dentomaxillofac Radiol* (2022) 10.1259/dmfr.20220044.

Keywords: ultrasonography; diagnostic imaging; periodontitis; gingiva; ultrasonic diagnosis

Introduction

Nearly 50% of Americans have periodontitis[1] resulting in pain, tooth loss,[2] reduced quality of life and even systemic effects like cardiovascular disease,[3] but tools to diagnose/monitor periodontitis have major limitations. Clinical assessment (by periodontal examination) and radiography are currently the standard of care but are time-consuming for the clinician, uncomfortable for the patient, and subject to large errors—interexaminer variation in probing can be >40%.[4] Moreover, clinical assessment and radiographic examination may not capture all clinical information (*e.g.*, gingival thickness and inflammation).

The periodontal examination provides critical information such as probing pocket depth (PPD; current

Correspondence to: Professor Casey Chen, E-mail: ccchen@usc.edu; Jesse V Jokerst, E-mail: jjokerst@ucsd.edu

Received 31 January 2022; revised 08 April 2022; accepted 11 April 2022; published online 09 May 2022
The authors Colman A Moore and Jane K Law contributed equally to the work.

periodontal health) and clinical attachment level (CAL; cumulative destruction).[5] PPD, CAL, and other clinical parameters form the basis of periodontal diagnosis. Radiography offers excellent sensitivity to hard tissue (bone, enamel, etc.) but cannot discriminate between healthy and diseased gingiva or map disease within soft tissue; it also has a small but non-negligible dose of ionizing radiation. Ultrasound imaging has the benefits of being a portable and low-cost alternative to radiography that is noninvasive and free of ionizing radiation. It can also resolve oral soft tissues including the gingiva and mucosa.

Locating the cementoenamel junction (CEJ) is important for determining metrics of periodontal health such as gingival recession and CAL. The CEJ is typically covered by the gingiva (subgingival), and its exact location is difficult to determine via physical probing and subject to significant error: In midbuccal sites, Vandana et al reported over- or underestimation of the CEJ by trained periodontists for 74% (34/46) of measured teeth.[6] Ultrasound has recently been used to directly image and identify the CEJ and other dental and periodontal structures.[7,8] Indeed, a rapidly expanding body of evidence has shown the translational value of ultrasonography for intraoral and dento-periodontal applications.[9–11] To briefly summarize, a variety of clinically relevant anatomical features have been visualized including the alveolar bone, CEJ, gingival thickness, greater palatine foramen, lingual nerve, and oral mucosa in healthy humans, *ex vivo* swine jaws, and cadavers.[7,8,12–15] Other reports have described computational approaches (*e.g.,* machine and deep learning) to automatically extract these features from imaging data.[16–18] Progress is also underway for improving the form factor and usability of transducer hardware and coupling materials[19,20]. However, ultrasonographic studies that incorporate orally diseased subjects are relatively nascent. Two recent examples include the use of power and color Doppler ultrasonography for measuring tissue perfusion/inflammation at dental implant sites and soft tissue grafts.[21,22] In a pilot study, Tattan et al reported strong agreement between ultrasound and direct/cone-beam computed tomography measurements of periodontal dimensions in a cohort of periodontally healthy subjects with a 24-MHz transducer.[23]

Here, we built upon this concept by using high-frequency (40-MHz) ultrasound to locate the CEJ in relation to other anatomical biomarkers (namely, the gingival margin (GM) and alveolar bone crest (ABC)) for image-based determination of periodontal metrics in periodontally healthy and diseased subjects. We compared these biomarkers to established clinical metrics of periodontal health. The central hypothesis of this study was that ultrasonographic imaging measurements could serve as a surrogate for clinical probing. To the best of our knowledge, this investigation is the first to report ultrasonographic determination of periodontal metrics in both healthy and diseased subjects for comparison with tandem clinical diagnosis.

Methods and materials

Materials

A high-frequency, commercially available imaging ultrasound system was employed (Vevo 2100/LAZR, Visualsonics, Toronto CA) using a linear array transducer (LZ-550, Fc = 40 MHz) with spatial resolution<200 µm.[24] Disposable tegaderm films were used as sterile transducer sleeves (3M, Minnesota, USA). Periodontal probing measurements were conducted with a Williams and Marquis probe.

Subject recruitment

The study protocol was approved by the USC and UCSD Institutional Review Boards and was in accordance with the ethical guidelines for human subjects research established by the Helsinki Declaration of 1975. The study subjects were identified from patients seeking dental care at the Herman Ostrow School of Dentistry. As part of the clinical protocol, the patients received extra- and intraoral examinations, medical and dental history review, a set of full-mouth radiographs, periodontal examination, periodontal diagnosis, and treatment planning. Eligible subjects were healthy adults who weighed at least 110 pounds with one quadrant with at least upper and lower anterior teeth. Subjects were excluded if they had bloodborne pathogen infections, bleeding disorders, acute oral infections, or were pregnant or lactating females. Two subject groups were recruited based on the periodontal diagnosis described in the 2017 World Workshop on the Classification of Periodontal and Peri-implant Diseases and Conditions.[25] The first group (n = 10) comprised subjects with the following diagnosis: periodontal health in intact or reduced periodontium in stable periodontitis patients, or dental biofilm-induced gingivitis in the intact or reduced periodontium. The second group (n = 6) comprised subjects diagnosed with periodontitis (Stage II-IV and Grade B or C) with localized or generalized involvement.

Clinical probing and diagnosis

The periodontal diagnosis was given by a board-certified periodontist faculty (K.C.J.C.) and a resident (J.L.). Six maxillary or mandibular anterior teeth were then selected for the study. We could not access molars because of the size of the transducer. Periodontal probing depth was determined with a Williams and Marquis probe at six sites per tooth (mesio-labial, mid-labial, disto-labial, mesio-lingual, mid-lingual, and disto-lingual). Tooth mobility was determined as Class 1: mobility of up to 1 mm in an axial direction, Class 2: mobility of greater than 1 mm in an axial direction, and Class 3: mobility in an apico-coronal

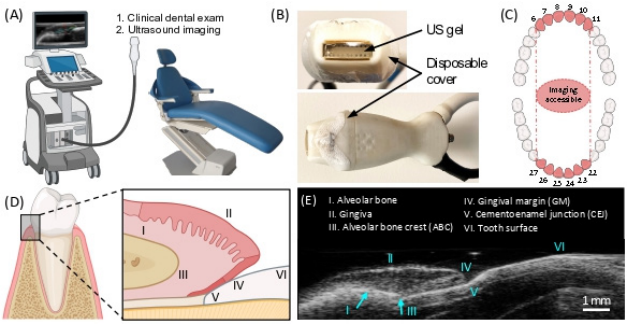

Figure 1 Overview of periodontal ultrasound imaging. (**A**) Schematic of chairside ultrasound imaging during routine dental examination. (**B**) Photograph of the commercial 40-MHz transducer with coupling gel and sterile sleeve used for subject imaging. (**C**)Dental chart with teeth highlighted (6-11, 22-27) that could be physically accessed by the ultrasound transducer. (**D**) Diagram of the periodontal anatomy surrounding the gingival sulcus with magnification of the sagittal plane. Roman numerals denote the I: alveolar bone, II: gingiva, III: alveolar bone crest (ABC), IV: gingival margin (GM), V: cementoenamel (CEJ), VI: tooth surface. (**E**) B-mode ultrasound image of the region in (F) for the central mandibular incisor (#25) of a patient with anatomical markers labeled.

direction (depressible tooth). Bleeding on probing (BOP) provoked by applying a probe to the bottom of the sulcus/pocket was recorded. Gingival recession was recorded by measuring the distance between the CEJ to the top of the gingival margin (GM) at the mid-labial position of the tooth with a periodontal probe. CAL was determined from the CEJ to the bottom of the sulcus. The gingival phenotype was determined by inserting the periodontal probe at the mid-labial sulcus of the tooth. A thin gingival phenotype was assigned if the probe was visible through the gingival tissue according to clinical convention.

Periodontal ultrasonography

A high-frequency, commercially available imaging system was used for chairside imaging of subjects (Figure 1A). Subjects were seated in the supine position in a dental chair and imaged by a clinician (Examiner 1) with a handheld, linear array transducer. A disposable sleeve was used to wrap the transducer in addition to sterile ultrasound coupling gel. Imaging was performed manually by positioning the transducer parallel to the long axis of the tooth along the labial midline. The handheld linear array transducer (40 MHz, Figure 1B) permitted access to the maxillary/mandibular incisors and cuspids (teeth 6–11 and 22–27, Figure 1C). B-mode images (2D ultrasound cross-sectional images) were collected in the sagittal plane at the mid-labial site of each tooth. The anatomy of the imaged region is depicted in Figure 1D for comparison to a representative B-mode image in Figure 1E. In general, six anatomical markers were consistently identified and used to orient the imaging operator: the alveolar bone, the gingiva, ABC, GM, CEJ, and the tooth surface.

Image analysis

Images were analyzed and measured manually. All images had to meet specific quality criteria by the examiner prior to measurement. These were: 1) identification of the GM, (2) identification of the ABC, and (3) a lack of interfering artifacts coincident with the relevant anatomy. If these conditions were met, then further image analysis was performed (Supplementary Appendix Table 1). All imaging measurements were performed in duplicate by two blinded examiners and averaged. The first was a clinician without prior ultrasound experience (Examiner 1) while the second was an ultrasound researcher (Examiner 2). Imaging measurements were performed digitally by each examiner in the VisualSonics software and ImageJ.[15,26] The distance from the GM to the ABC was defined as the image-based gingival height (iGH). Similarly, the distance from the CEJ to the ABC was defined as the image-based alveolar bone level (iABL). The image-based gingival thickness (iGT) was measured at the midpoint of the ABC and GM.

Statistical analysis

The suitability of sample size for determining measurement differences between teeth grouped as periodontally healthy or diseased was estimated via power analysis for a two-tailed significance test with 95% significance ($\alpha = 0.05$), 80% power ($\beta = 0.20$), variance = 0.3 mm^2, and minimum differences of 0.4, 0.5, or 1.0 mm (Supplementary Appendix Figure 1). Bland-Altman analysis was performed to quantify differences (bias, limits of agreement) between image examiners and between physical probing and imaging measurements. Box-and-whisker plots were combined with unpaired, two-tailed significance testing ($\alpha = 0.05$) to compare healthy and diseased groups of measured/imaged teeth. Analysis was performed with GraphPad Prism 9 (San Diego, CA) and Microsoft Excel (Redmond, Washington).

Results

In humans, 79 B-mode images were acquired from 16 subjects comprising 43 teeth clinically diagnosed as healthy and 36 diagnosed with periodontal disease via physical measurements and examination. Of these images, 66 (84%) met quality criteria and were used for analysis. All image quality metrics, image measurements, and clinical measurements are included in Supplementary Appendix Table 1.

One simple periodontal measurement is the distance between the CEJ and GM, which is used to assess gingival migration (recession or overgrowth). To demonstrate this with ultrasonography, Figure 2 shows varying positions of the CEJ relative to the GM for six different subjects. The CEJ presents as an angled disruption in the echogenicity of the tooth surface between the GM and ABC. For subjects in Figure 2A–C, the CEJ is

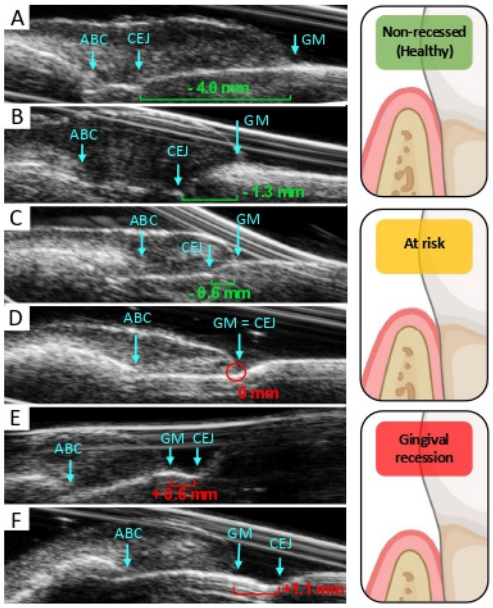

Figure 2 B-mode images in six subjects demonstrating ultrasound monitoring of gingival recession via periodontal landmarks. Clinically, the distance between the CEJ and GM defines the extent of gingival recession and is used to determine CAL. Panels **A-F**) show teeth from subjects with increasing levels of gingival recession. (**A-C**) Images from subjects with the CEJ apical to the GM (*i.e.,* non-recessed). These measurements are represented as negative values (green). (**D**) Image from a subject where the GM is coincident with the CEJ (*i.e.,* PPD = CAL). (**E-F**) Images from subjects with the GM apical to the CEJ (*i.e.,* recessed). Recessed measurements are represented as positive values (red).

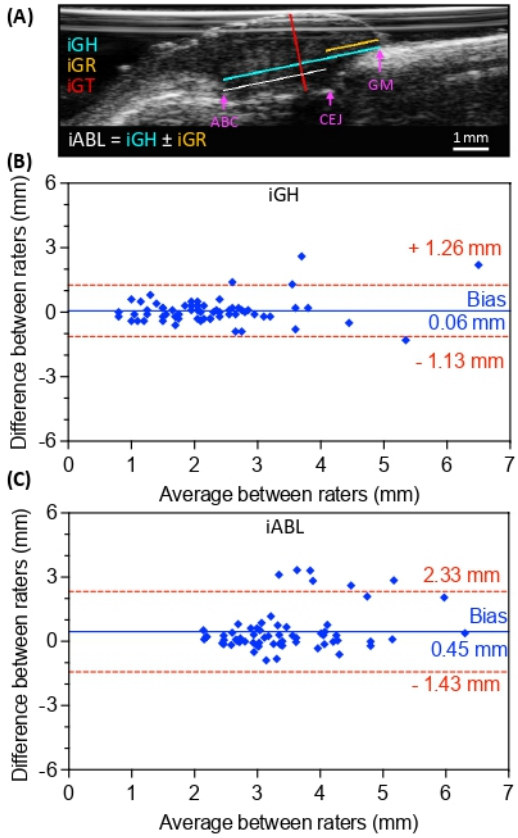

Figure 3 Ultrasound for diagnostic measurements and interexaminer variability for ultrasound image-based measurements of pocket depth (iPD) and clinical attachment level (iCAL). (**A**) B-mode image with manual annotations showing the extraction of iGH (teal), iABL (white), iGR (yellow), and iGT (red) for a representative subject. The iGH is defined as the distance from the ABC to the GM. (**B-C**) Bland-Altman plots comparing the iGH and iABL measurements from two blinded image analysts for the same image set (n = 66 teeth). The increased variance (bias) between analysts for iABL (0.45 ± 0.96 mm) relative to iGH (0.06 ± 0.61 mm) was due to differences in identification of the CEJ between the two image analysts.

apical to the GM (typically, a positive health marker) showing subgingival CEJ-GM distances of −4.0 mm, −1.3 mm, and −0.6 mm. The CEJ and GM are coincident in Figure 2D. The last two cases have gingival recession (Figure 2E–F)**:** The GM is apical to the CEJ (0.6 mm and 1.1 mm, respectively).

All image-based measurements including iGH, iABL, iGT, and iGR (image-based gingival recession), are depicted for a representative tooth site in Figure 3A. To determine the iGH and iABL values in this study, two blinded examiners independently measured each B-mode image and their values were averaged. Bias between raters was <0.1 mm for iGH (Figure 3B) and 0.45 mm for iABL (Figure 3C). The average iGH and iABL values for teeth from healthy/diseased subjects were compared to clinical PPD and CAL measurements, respectively (Figure 4). The average PPD measurements were 1.68 mm for healthy subjects and 2.25 mm for diseased subjects (Figure 4A). A similar increase was observed for iGH measurements: 3.19 mm for healthy subjects and 3.67 mm for diseased subjects (Figure 4A). In both cases, measurements in diseased subjects were significantly higher than in healthy subjects (unpaired, two-tailed t-test, p = 0.0142 for PPD, p = 0.0286 for iGH). Expectedly, iGH values were larger than PPD values (1.57 mm Bland-Altman bias, on average) because the iGH measurements terminated at the ABC rather than the gingival sulcus (Figure 4B). As with the PPD measurements, CAL measurements were significantly higher for diseased than healthy subjects: 1.68 mm in the healthy group and 2.56 mm in the diseased group (unpaired, two-tailed t-test, p = 0.0003, Figure 4C). For iABL, the healthy average was 1.80 mm, and the diseased average was 2.74 mm—this difference between groups was even more significant than the CAL measurements (p < 0.0001, Figure 4C). Bland-Altman analysis indicated a minor 0.25 mm magnitude bias toward iABL measurements relative to CAL (Figure 4D). Overall, the average increases in magnitude of PPD, iGH, CAL, and iABL for diseased versus healthy teeth were 34%, 15%, 52%, and 52%, respectively.

In our dataset, the average difference between iGH and PPD measurements was 1.57 mm. Defining this value as the average biologic width[28] and subtracting it from each iGH measurement, we obtained a set of iPD values after rounding to the nearest integer similar to

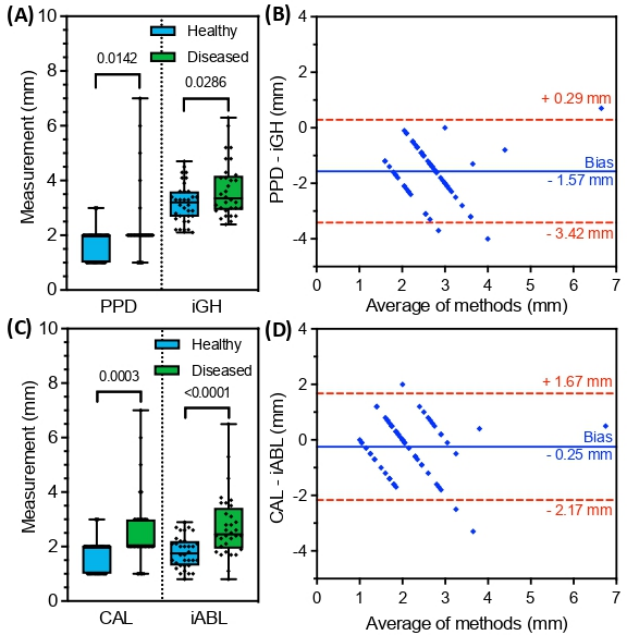

Figure 4 Comparison between ultrasound image-based measurements (iGH, iABL) and clinical probing measurements (PPD, CAL) for individual teeth (n = 66) of patients with healthy or diseased clinical diagnoses. (**A**) Box-and-whisker plots for PPD and iGH both indicate significantly higher measurements in the diseased group (n = 32) than the healthy group (n = 34); PPD values are limited to integers. Pairwise comparison values are p-values (unpaired, two-tailed t-test). (**B**) Bland-Altman analysis between the measurement methods shows a 1.57 ± 0.95 mm bias toward iGH measurements averaged from all teeth– these values are larger because—while both measurements begin at the GM—the iGH is measured to the ABC rather than the terminus of the gingival sulcus. This difference, due to the connective tissue and junctional epithelium between the ABC and gingival sulcus, has been described as the "biological width".[27] (**C**) Box-and-whisker plots for iABL and CAL indicate significantly higher values for teeth in the diseased group than the healthy group. CAL values are limited to integers. Pairwise comparison values are p-values (unpaired, two-tailed t-test). (**D**) Bland-Altman analysis between the iABL/CAL measurement methods reveal a 0.25 ± 0.98 mm bias toward the iABL measurements indicating a minimal difference between the two methods.

the rounding done when measuring the PPD. Likewise, we obtained a set of iCAL values after performing the same subtraction from the iABL data. This analysis led to 83% agreement between iPD and PPD values, and 49% agreement between iCAL and CAL values; here, agreement was defined as ≤1 mm difference between paired measurements. Lastly, iGT was compared to gingival biotype: 93.5% of the associated gingiva for measured teeth possessed a thick biotype, and there was no correlation to disease status (Supplementary Appendix Figure 2A). Accordingly, the iGT measurements (taken from the midpoint of the ABC and GM) were not significantly different for healthy versus diseased patients (Supplementary Appendix Figure 2B).

Discussion

The CEJ and the GM are two of the most prominent features in ultrasound images at mid-labial sites (Figure 1E). These can be used to precisely measure the extent of gingival recession or overgrowth (Figure 2), which is otherwise an error-prone estimate using periodontal probing. We envision that the ability to resolve the CEJ quickly and objectively in relation to the GM using chairside and handheld transducers will enable more accurate and higher throughput longitudinal monitoring of gingival recession than standard probing. Of course, gingival recession alone does not provide a full picture of periodontal health because it is often multifactorial in origin.[29,30] Therefore, we investigated the value of measurements derived from the CEJ, GM, and ABC as diagnostic gingival biomarkers, i.e., iGH and iABL (Figure 3A). Interexaminer bias values from Bland-Altman analysis were acceptably low for both iGH (0.06 mm) and iABL (0.45 mm) (Figure 3B–C) because these are lower than the precision of clinical probing which is restricted to integer measurements. The increased difference for iABL arose from differences between the examiners in assigning the CEJ, which can be a less obvious feature than the ABC or GM.

We found that sonography alone—even at high frequency (40 MHz in this study)—cannot resolve the periodontal pocket or depth of the gingival sulcus directly via endogenous contrast. This is likely because the free (unattached) gingiva that forms the sulcus remains conformal with the tooth surface, thus rendering it indistinguishable via endogenous imaging from attached gingiva. Nevertheless, iGH and iABL were effective surrogate measurements for PPD and CAL as illustrated by their similarly increased magnitudes for periodontally diseased *vs* healthy teeth (Figure 4). We compared iGH to PPD and iABL to CAL because these measurements are physically equivalent except for their termini—i.e., the iGH and iABL terminate at the ABC while the PPD and CAL terminate at the apex of the gingival sulcus. This difference—the distance between the ABC and the terminus of the gingival sulcus (corresponding to connective tissue and junctional epithelium)—has been described as the "biologic width".[28] While our measured estimate for the biologic width (1.57 mm) falls within the range of mean values reported in a systematic meta-analysis (between 1.15–3.95 mm), the disease state, tooth type, probing depth, and attachment loss can all of course affect the biological width.[27] The combination of these variables and the lack of precision in locating the subgingival CEJ with a periodontal probe are likely reasons for the relatively low agreement between iCAL and CAL values in this study (49%). Given the higher accuracy of physical probing for PPD measurements, the comparison between iPD and PPD is both more reliable and promising with 83% agreement. Importantly, while recapitulating the PPD values via imaging has value, the iGH

and iABL are simpler metrics and do not require *a priori* estimation of the biologic width. Treating the biologic width as a correction factor is useful to help correlate these gingival biomarkers to conventional metrics of periodontal health; however, it is possible to imagine them being used independent of conventional probing measurements. Of course, the full clinical value will need to be validated with larger cohorts of diseased subjects that include molars and premolars because these teeth typically have deeper pockets but could not be imaged in this study due to the size of the transducer.

Ultrasound can also measure gingival thickness with a high degree of precision and accuracy—while iGT alone does not reflect periodontal health, it is an important metric in the context of operations such as gum grafts and periodontal flap surgeries. Currently, biotype is a binary evaluation performed by inserting the periodontal probe into the gingival sulcus and assessing probe visibility. A visible probe corresponds to a "thin" biotype and an invisible probe corresponds to a "thick" biotype. Actual values for thin and thick biotypes have been proposed as <1.0 mm GT and >1.0 mm GT, respectively.[31] We did not observe a statistical difference between GT or iGT measurements in healthy and diseased patients (Supplementary Appendix Figure 2B). Although imaging is significantly more precise than the probe visibility method, this comparison served as assurance that iGT measurements were not biased by the health status of the patient.

The imaging technique faced a few limitations. In our dataset, 16% of the acquired images could not be included for analysis (Supplementary Appendix Table 1) because the images contained interfering artifacts from imperfect coupling or transducer positioning (*e.g.,* bubbles, acoustic reflections). These artifacts were primarily generated by the specific geometry of the transducer, *i.e.,* the ~0.5 cm gap between the transducer elements and the tissue surface— fortunately, many transducers do not have this gap. However, in handheld ultrasonography, operator experience also plays a role, particularly for judging image quality as the imaging is being performed (*i.e.,* in real time). The operator in this study was a dental clinician without prior background in performing ultrasonography. Future clinical scenarios will include a more formalized training program or simply leverage more experience in recognizing echogenic landmarks that can improve the pass rate. Another challenge was the size of the transducer (5 cm width). This restricted imaging to the labial surfaces of teeth 6–11 and 22–27. The ideal transducer could access the buccal and lingual surfaces of the full dentition. Practical clinical deployment will also need to integrate computational techniques to automatically extract imaging biomarkers.[16,17,32,33] Nevertheless, ultrasound may have significant clinical value for longitudinal monitoring of periodontal health. Unlike other oral imaging modalities, ultrasonography offers details of both hard and soft tissues, thus facilitating the measurement of periodontal metrics that require the resolution of both hard (ABC, CEJ) and soft (GM, GT) features. It is non-ionizing, painless, and can be operated chairside with minimal training.

Conclusions

We investigated the use of high-frequency ultrasound in 10 healthy subjects (34 teeth) and 6 subjects with periodontal disease (32 teeth) for measuring critical metrics of periodontal health, including probing pocket depth, clinical attachment level, gingival recession, and gingival thickness at mid-labial sites. Image-based measurements of gingival height extended from the gingival margin to the alveolar bone crest and were comparable to probing pocket depth (1.57 mm magnitude bias) with functional equivalence for assessing disease status. Identification of the cementoenamel junction by human operators also allowed image-based measurement of alveolar bone level and gingival recession. Interexaminer bias was negligible (<0.1 mm) for gingival height and 0.45 mm for alveolar bone level measurements. Image-based alveolar bone level measurements were equivalent to clinical attachment level for staging disease (0.25 mm magnitude bias). Overall, ultrasonographic metrics had at least an equivalent diagnostic capacity to gold-standard physical probing while offering more detailed anatomical information and painless operation. We anticipate that advances in the form factor of high-frequency transducers will facilitate the further translation of ultrasonography into the dental clinic.

Acknowledgment

The project was partially supported by the National Institutes of Health, Grants UL1TR001442, R21 DE029025, and R21 DE029917. The content is solely the responsibility of the authors and does not necessarily represent the official views of the NIH. The work was supported in part by the National Science Foundation Graduate Research Fellowship Program under Grant No. DGE-1650112. C.M. graciously acknowledges support from the ARCS Foundation. Figure 1 was created in part with BioRender.

Conflict of interests

Colman A. Moore, Jane K. Law, Maurice Retout, Christopher T. Pham, Kai Chiao J. Chang, and Casey Chen report no conflicts of interest related to this study. Jesse V. Jokerst is a co-founder of StyloSonics, LLC.

DISCLOSURES

Jesse V. Jokerst is a co-founder of StyloSonic, LLC.

REFERENCES

1. Eke PI, Dye BA, Wei L, Thornton-Evans GO, Genco RJ, CDC Periodontal Disease Surveillance workgroup: James Beck (University of North Carolina, Chapel Hill, USA), Gordon Douglass (Past President, American Academy of Periodontology), Roy Page (University of Washin. Prevalence of periodontitis in adults in the united states: 2009 and 2010. *J Dent Res* 2012; **91**: 914–20. https://doi.org/10.1177/0022034512457373
2. Brennan DS, Spencer AJ, Roberts-Thomson KF. Tooth loss, chewing ability and quality of life. *Qual Life Res* 2008; **17**: 227–35. https://doi.org/10.1007/s11136-007-9293-2
3. Tonetti MS, Van Dyke TE, Working group 1 of the joint EFP/AAP workshop. Periodontitis and atherosclerotic cardiovascular disease: consensus report of the joint EFP/AAP workshop on periodontitis and systemic diseases. *J Clin Periodontol* 2013; **40 Suppl 14**: S24-9. https://doi.org/10.1111/jcpe.12089
4. Grossi SG, Dunford RG, Ho A, Koch G, Machtei EE, Genco RJ. Sources of error for periodontal probing measurements. *J Periodontal Res* 1996; **31**: 330–36. https://doi.org/10.1111/j.1600-0765.1996.tb00500.x
5. . Perry DA, Beemsterboer PL, Essex G. Periodontology for the dental hygienist. Elsevier Health Sciences; 2015.
6. Vandana KL, Gupta I. The location of cemento enamel junction for CAL measurement: A clinical crisis. *J Indian Soc Periodontol* 2009; **13**: 12–15. https://doi.org/10.4103/0972-124X.51888
7. Izzetti R, Vitali S, Aringhieri G, Oranges T, Dini V, Nisi M, et al. Discovering a new anatomy: exploration of oral mucosa with ultra-high frequency ultrasound. *Dentomaxillofac Radiol* 2020; **49**(7): 20190318. https://doi.org/10.1259/dmfr.20190318
8. Nguyen K-C, Le LH, Kaipatur NR, Major PW. Imaging the cemento-enamel junction using a 20-mhz ultrasonic transducer. *Ultrasound Med Biol* 2016; **42**: 333–38. https://doi.org/10.1016/j.ultrasmedbio.2015.09.012
9. Ultrasound for Periodontal Imaging. In: *Dental Ultrasound in Periodontology and Implantology: Examination, Diagnosis and Treatment Outcome Evaluation*. Cham: Springer International Publishing; 2021, pp. 115–29.
10. Chan H-L, Kripfgans OD. (n.d.). *Dental Ultrasound in Periodontology and Implantology*. Cham: Springer, pp.161–75. https://doi.org/10.1007/978-3-030-51288-0
11. Bhaskar V, Chan H-L, MacEachern M, Kripfgans OD. Updates on ultrasound research in implant dentistry: a systematic review of potential clinical indications. *Dentomaxillofac Radiol* 2018; **47**(6): 20180076. https://doi.org/10.1259/dmfr.20180076
12. Sinjab K, Kripfgans OD, Ou A, Chan H-L. Ultrasonographic evaluation of edentulous crestal bone topography: A proof-of-principle retrospective study. *Oral Surg Oral Med Oral Pathol Oral Radiol* 2022; **133**: 110–17. https://doi.org/10.1016/j.oooo.2021.07.006
13. Chifor R, Radu C, Badea ME, Eugenia BM, Hedesiu M, Mihaela H, et al. Experimental model for measuring and characterisation of the dento-alveolar system using high frequencies ultrasound techniques. *Med Ultrason* 2010; **12**: 127–32.
14. Chifor R, Badea AF, Chifor I, Mitrea D-A, Crisan M, Badea ME. Periodontal evaluation using a non-invasive imaging method (ultrasonography). *Med Pharm Rep* 2019; **92**: S20–32. https://doi.org/10.15386/mpr-1521
15. Chan H-L, Wang H-L, Fowlkes JB, Giannobile WV, Kripfgans OD. Non-ionizing real-time ultrasonography in implant and oral surgery: A feasibility study. *Clin Oral Implants Res* 2017; **28**: 341–47. https://doi.org/10.1111/clr.12805
16. Nguyen KCT, Duong DQ, Almeida FT, Major PW, Kaipatur NR, Pham TT, et al. Alveolar bone segmentation in intraoral ultrasonographs with machine learning. *J Dent Res* 2020; **99**: 1054–61. https://doi.org/10.1177/0022034520920593
17. Nguyen K-C, Le BM, Li M, Almeida FT, Major PW, Kaipatur NR, et al. Localization of cementoenamel junction in intraoral ultrasonographs with machine learning. *J Dent* 2021; **112**: 103752. https://doi.org/10.1016/j.jdent.2021.103752
18. Pan Y-C, Chan H-L, Kong X, Hadjiiski LM, Kripfgans OD. Multi-class deep learning segmentation and automated measurements in periodontal sonograms of a porcine model. *Dentomaxillofac Radiol* 2021; **50**: 20210363.
19. Yi J, Nguyen K-C, Wang W, Yang W, Pan M, Lou E, et al. Polyacrylamide/alginate double-network tough hydrogels for intraoral ultrasound imaging. *J Colloid Interface Sci* 2020; **578**: 598–607. https://doi.org/10.1016/j.jcis.2020.06.015
20. Chifor R, Li M, Nguyen K-CT, Arsenescu T, Chifor I, Badea AF, et al. Three-dimensional periodontal investigations using a prototype handheld ultrasound scanner with spatial positioning reading sensor. *Med Ultrason* 2021; **23**: 297–304. https://doi.org/10.11152/mu-2837
21. Tavelli L, Barootchi S, Majzoub J, Chan H-L, Giannobile WV, Wang H-L, et al. Ultrasonographic tissue perfusion analysis at implant and palatal donor sites following soft tissue augmentation: A clinical pilot study. *J Clin Periodontol* 2021; **48**: 602–14. https://doi.org/10.1111/jcpe.13424
22. Barootchi S, Tavelli L, Majzoub J, Chan HL, Wang HL, Kripfgans OD. Ultrasonographic tissue perfusion in peri-implant health and disease. *J Dent Res* 2022; **101**: 278–85. https://doi.org/10.1177/00220345211035684
23. Tattan M, Sinjab K, Lee E, Arnett M, Oh T-J, Wang H-L, et al. Ultrasonography for chairside evaluation of periodontal structures: a pilot study. *J Periodontol* 2020; **91**: 890–99. https://doi.org/10.1002/JPER.19-0342
24. Moran CM, Pye SD, Ellis W, Janeczko A, Morris KD, McNeilly AS, et al. A comparison of the imaging performance of high resolution ultrasound scanners for preclinical imaging. *Ultrasound Med Biol* 2011; **37**: 493–501. https://doi.org/10.1016/j.ultrasmedbio.2010.11.010
25. Caton JG, Armitage G, Berglundh T, Chapple ILC, Jepsen S, Kornman KS, et al. A new classification scheme for periodontal and peri-implant diseases and conditions - introduction and key changes from the 1999 classification. *J Periodontol* 2018; **89 Suppl 1**: S1–8. https://doi.org/10.1002/JPER.18-0157
26. Moore C, Bai Y, Hariri A, Sanchez JB, Lin C-Y, Koka S, et al. Photoacoustic imaging for monitoring periodontal health: A first human study. *Photoacoustics* 2018; **12**: 67–74. https://doi.org/10.1016/j.pacs.2018.10.005
27. Schmidt JC, Sahrmann P, Weiger R, Schmidlin PR, Walter C. Biologic width dimensions--a systematic review. *J Clin Periodontol* 2013; **40**: 493–504. https://doi.org/10.1111/jcpe.12078
28. Nugala B, Kumar BS, Sahitya S, Krishna PM. Biologic width and its importance in periodontal and restorative dentistry. *J Conserv Dent* 2012; **15**: 12–17. https://doi.org/10.4103/0972-0707.92599
29. Bahal P, Malhi M, Shah S, Ide M. Managing the consequences of periodontal diseases/treatment: gingival recession. *Dent Update* 2019; **46**: 966–77. https://doi.org/10.12968/denu.2019.46.10.966
30. Tugnait A, Clerehugh V. Gingival recession-its significance and management. *J Dent* 2001; **29**: 381–94. https://doi.org/10.1016/s0300-5712(01)00035-5
31. Alves PHM, Alves TCLP, Pegoraro TA, Costa YM, Bonfante EA, de Almeida ALPF. Measurement properties of gingival biotype evaluation methods. *Clin Implant Dent Relat Res* 2018; **20**: 280–84. https://doi.org/10.1111/cid.12583
32. Ilhan B, Guneri P, Wilder-Smith P. The contribution of artificial intelligence to reducing the diagnostic delay in oral cancer. *Oral Oncol* 2021; **116**: 105254. https://doi.org/10.1016/j.oraloncology.2021.105254
33. Daniels K, Gummadi S, Zhu Z, Wang S, Patel J, Swendseid B, et al. Machine learning by ultrasonography for genetic risk stratification of thyroid nodules. *JAMA Otolaryngol Head Neck Surg* 2020; **146**: 36–41. https://doi.org/10.1001/jamaoto.2019.3073